THE JOURNAL OF BIOLOGICAL CHEMISTRY VOL. 286, NO. 51, pp. 43717–43725, December 23, 2011

Junctophilin 1 and 2 Proteins Interact with the L-type Ca^{2+} Channel Dihydropyridine Receptors (DHPRs) in Skeletal Muscle*[S]

Received for publication, August 12, 2011, and in revised form, October 18, 2011 Published, JBC Papers in Press, October 21, 2011, DOI 10.1074/jbc.M111.292755

Lucia Golini[‡1], Christophe Chouabe[§1], Christine Berthier[§], Vincenza Cusimano[‡], Mara Fornaro[‡2], Robert Bonvallet[§], Luca Formoso[‡], Emiliana Giacomello[‡], Vincent Jacquemond[§], and Vincenzo Sorrentino[‡3]

From the [‡]Molecular Medicine Section, Department of Neuroscience, and Interuniversity Institute of Myology, University of Siena, 53100 Siena, Italy and the [§]Centre de Génétique et de Physiologie Moléculaire et Cellulaire, Université Lyon 1, UMR CNRS 5534, 69622 Villeurbanne cedex, France

Background: Junctophilins form junctional membrane complexes between the sarcoplasmic reticulum and the plasma membrane in skeletal muscle.
Results: Junctophilins interact with both the dihydropyridine receptors and the ryanodine receptor Ca^{2+} channels.
Conclusion: Assembly of junctional proteins in junctional membrane complexes is facilitated by Junctophilins.
Significance: This suggests that junctophilins have multiple roles in the assembly of Ca^{2+} release units in muscle cells.

Junctophilins (JPs) anchor the endo/sarcoplasmic reticulum to the plasma membrane, thus contributing to the assembly of junctional membrane complexes in striated muscles and neurons. Recent studies have shown that JPs may be also involved in regulating Ca^{2+} homeostasis. Here, we report that in skeletal muscle, JP1 and JP2 are part of a complex that, in addition to ryanodine receptor 1 (RyR1), includes caveolin 3 and the dihydropyridine receptor (DHPR). The interaction between JPs and DHPR was mediated by a region encompassing amino acids 230–369 and amino acids 216–399 in JP1 and JP2, respectively. Immunofluorescence studies revealed that the pattern of DHPR and RyR signals in C2C12 cells knocked down for JP1 and JP2 was rather diffused and characterized by smaller puncta in contrast to that observed in control cells. Functional experiments revealed that down-regulation of JPs in differentiated C2C12 cells resulted in a reduction of intramembrane charge movement and the L-type Ca^{2+} current accompanied by a reduced number of DHPRs at the plasma membrane, whereas there was no substantial alteration in Ca^{2+} release from the sterol regulatory element-binding protein. Altogether, these results suggest that JP1 and JP2 can facilitate the assembly of DHPR with other proteins of the excitation-contraction coupling machinery.

The sarcoplasmic reticulum (SR)[4] of skeletal muscle cells is a highly specialized form of the smooth endoplasmic reticulum that controls Ca^{2+} storage and release to regulate muscle contraction (1, 2). Activation of Ca^{2+} release from the SR is linked to depolarization of the plasma membrane in a process named excitation-contraction (e-c) coupling (3). In skeletal muscle, e-c coupling requires the close association of two membrane compartments: the transverse tubules (T-tubules), which are invaginations of the plasma membrane, and the terminal cisternae, which are specialized domains of SR, resulting in the formation of junctional membrane complexes, also known as triads. Junctional membrane complexes are enriched in proteins participating in the e-c coupling mechanism and therefore can be observed by immunofluorescence staining with selective antibodies as transverse striations localized corresponding to the junction between the A-I bands in mature mammalian skeletal muscle fibers, whereas in cultured myotubes, they appear as clusters or puncta distributed in a more irregular way with respect to the contractile apparatus (1). Two major proteins are known to play an important role in signaling between the T-tubule and the terminal cisternae of SR: the dihydropyridine receptor (DHPR) and the ryanodine receptor (RyR). The DHPR, on the T-tubule membrane, is the voltage-gated Cav1.1 L-type channel, consisting of five subunits (4, 5), that functions as a voltage sensor in the e-c coupling mechanism, whereas the RyR is a high conductance tetrameric Ca^{2+} release channel, located on the membrane of the terminal cisternae of the SR (3). In mature skeletal muscle, e-c coupling critically depends on the direct interaction between RyR1 and DHPR. Activation of DHPR by membrane depolarization induces conformational changes and opening of RyR1, leading to release of Ca^{2+} from the lumen of SR into the cytoplasm and muscle contraction (3, 6).

Although the molecular mechanisms responsible for the formation and organization of junctional membrane complexes are still not completely understood, some of the proteins responsible for their formation during muscle development

* This work was supported in part by a grant from Telethon (GGP08153).
[S] The on-line version of this article (available at http://www.jbc.org) contains supplemental Methods and Figs. S1 and S2.
[1] Both authors contributed equally to this work.
[2] Present address: Novartis Institutes for Biomedical Research, Forum 1, Novartis Campus, 4056 Basel, Switzerland.
[3] To whom correspondence should be addressed: Molecular Medicine Section, Dept. of Neuroscience, University of Siena, via A. Moro, 53100 Siena, Italy. Tel.: 39-0577-234-079; Fax: 39-0577-234-191; E-mail: vincenzo.sorrentino@unisi.it.
[4] The abbreviations used are: SR, sarcoplasmic reticulum; ER, endoplasmic reticulum; e-c, excitation-contraction; JP, junctophilin; RyR, ryanodine receptor; DHPR, dihydropyridine receptor; T-tubule, transverse tubule; TRPC, transient receptor potential channel; TEA, triethanolamine; TTX, tetrodotoxin; aa, amino acids; F, farads.

have been identified (7). Junctophilins (JPs) are a class of highly conserved proteins that are localized at junctional membrane complexes and are involved in anchoring the endo/sarcoplasmic (ER/SR) membranes to the sarcolemma/T-tubules. JPs are composed of a large cytoplasmic region and a carboxyl-terminal hydrophobic transmembrane segment spanning the junctional ER/SR membranes. The cytoplasmic region of JPs contains the repeated motifs of 14 amino acid residues, named "MORN motifs," that exhibit selective binding affinity to the plasma membrane (8). The four known junctophilin genes (JP1, JP2, JP3, and JP4) are differentially expressed throughout excitable cells; both JP1 and JP2 are expressed in skeletal muscle, JP2 is the only isoform expressed in cardiac and smooth muscle, whereas neurons express both JP3 and JP4 (7, 9–12). In skeletal muscle, the expression and proper targeting of JP1 appear to be involved in the correct formation and stabilization of triads. Heterologous expression of JP1 in amphibian embryos results in formation of artificial plasma membrane/ER junctions, whereas JP1 knock-out mice show neonatal lethality and disrupted membrane junctional structures in skeletal muscle fibers with limited muscle contraction (9, 12, 13). Knock-out of JP2 caused an increase in the gap between plasma membrane and the junctional SR and altered Ca^{2+} signaling in cardiomyocytes, resulting in embryonic lethality (7). More recent studies on JPs have identified missense mutations in JP2 in patients with hypertrophic cardiomyopathy (14, 15), and decreased levels of JP2 expression have been reported in animal models of aortic stenosis (16) and hypertrophic and dilated cardiomyopathy (17). In addition, patients with hypertrophic cardiomyopathy presented reduced levels of JP2 expression associated with reduced excitation-contraction coupling gain as well as altered Ca^{2+} homeostasis (14). Comparable alterations were reported in knockdown mice with reduced JP2 expression (18). Altogether, these evidences strongly suggest that JP1 and JP2 have a critical role in the assembly of the junctional membrane complexes that support the e-c coupling mechanism.

Furthermore, Phimister *et al*. (19) reported that JP1 and RyR1 interact in a conformation-sensitive manner that coincides with changes in the reactivity of specific thiol residues residing on both proteins. An interaction between JP2 and RyR2 has been reported by van Oort *et al.* (18). Additional evidence has suggested that JPs could interact with other proteins that control Ca^{2+} homeostasis and e-c coupling. JP1 was shown to be up-regulated in myotubes expressing low levels of TRPC3 (20), a Ca^{2+}-permeant channel interacting directly with JP2 (21, 22) and presumed to also be functionally linked to RyR1 in muscle (20, 21). Conversely, JP1-deficient muscle cells yield a reduced expression of TRPC3 as well as changes in expression of other channels from the TRPC family (23). Although the role of TRPC channels in muscle remains misunderstood (24, 25), available results highlight the existence of complex interactions between this class of Ca^{2+}-permeant channels, JPs, and ryanodine receptors. Junctophilin deficiency in muscle cells was also reported to be associated with compromised store-operated calcium entry (26) and with reduced normal resting Ca^{2+} entry (23). The identity of the molecules responsible for these Ca^{2+} entry pathways in muscle remains controversial, but there is growing evidence for a significant contribution of the STIM1-Orai1 protein system (23, 27, 28). Interestingly, both components of this mechanism were found down-regulated in JP1-deficient myotubes (23), suggesting that JP1 may be an important determinant of proper function of STIM1-Orai-1-mediated resting- and store-operated- trans-plasma membrane Ca^{2+} entry. Also worth mentioning in this context is the recently discovered possibility of interactions between STIM1 and voltage-gated Ca^{2+} entry, as demonstrated for Cav1.2 channels (29, 30).

Here, we report data from immunoprecipitation and pull-down experiments showing that in skeletal muscle, JP1 and JP2 can be found in a macromolecular complex that includes RyR1, Cav3, and the DHPR. Immunostaining experiments revealed that the DHPR and RyR signals in C2C12 cells following knockdown of JP1 and JP2 were significantly more diffused than those observed in control cells. Functional experiments showed that knockdown of JPs in cultured myotubes reduced the density of L-type Ca^{2+} current and intramembrane charge movement with no concurrent alteration of SR Ca^{2+} release.

EXPERIMENTAL PROCEDURES

Microsome Preparation and Solubilization—Microsomes from rabbit skeletal muscle were prepared as described previously (31) and stored at −80 °C until use or solubilized with a lysis buffer containing 1% Triton X-100, 10 mM Tris, pH 7.4, 150 mM NaCl, 5 mM EDTA, 1 mM Na_3VO_4, 10% glycerol, 1× protease inhibitor for 3 h at 4 °C and centrifuged for 30 min at 100,000 × *g* to remove insoluble proteins.

Cell Cultures—HEK293-T cells were grown at 37 °C under 5% CO_2 in α-MEM containing 10% heat-inactivated fetal bovine serum (Bio-Whittaker). C2C12 myoblasts were maintained in DMEM medium supplemented with 10% heat-inactivated fetal calf serum at 37 °C. The day before transfection, the cells were split and seeded onto gelatin-coated coverslips. Cells were then transfected with the appropriated plasmid by means of Lipofectamine Plus reagent and induced to differentiate in DMEM supplemented with 2% horse serum until the appearance of differentiated myotubes.

Immunofluorescence—Cells were fixed with 3% paraformaldehyde and permeabilized with Hepes-Triton buffer (20 mM Hepes, pH 7.4, 300 mM sucrose, 50 mM NaCl, 3 mM $MgCl_2$, 0.5% Triton X-100). For immunofluorescence experiments, cells were blocked with 0.2% BSA and 5% goat or fetal calf serum in PBS and incubated with primary antibodies overnight. The cells were extensively washed with 0.2% PBS-BSA and incubated with Cy2 or Cy3 conjugated secondary antibodies (Jackson ImmunoResearch Laboratories) for 1 h at room temperature, washed with 0.2% PBS-BSA, and mounted with Mowiol added with 0.025% 1,4-diazabicyco [2,2,2] octane as antifading agent. The specimens were analyzed with a confocal microscope (LSM510, Zeiss, Jena, Germany). Fluorescence measurements were performed by means of ImageJ software by measuring the total mean fluorescence intensity of sets of transfected and non-transfected cells imaged in the same field. Similarly, the size of puncta was calculated by means of the ImageJ "analyze particles" function in transfected and non-transfected cells. A limit of 0.163 μm^2 was fixed to subdivide puncta into small ($<$ 0.163) and large ($>$0.163) puncta. For calculating the frequency

of small and large puncta, a total of 7152 puncta were analyzed in C2C12 cells knocked down for JP1 and JP2 and a total of 5730 from C2C12 cells transfected with the control vector.

Co-immunoprecipitation—Solubilized proteins from skeletal muscle microsomes or from HEK293-T cells were precleared with protein G-Sepharose or protein A-Sepharose beads (Amersham Biosciences) for 30 min at 4 °C. 100 μg of precleared solubilized proteins were incubated overnight at 4 °C, with the specific antibodies. Afterward the complexes were diluted (5×) in lysis buffer and incubated with protein G-Sepharose or protein A-Sepharose beads for 4 h. Beads were washed four times with lysis buffer to remove nonspecifically bound proteins. The immune complexes were treated with sample buffer and analyzed with sodium dodecyl sulfate-polyacrylamide gel electrophoresis (SDS-PAGE).

SDS-PAGE and Immunoblotting—The samples were subjected to 10% SDS-PAGE for 1 h and 30 min at 25 mA, transferred to PVDF membranes (Millipore), and incubated overnight at 4 °C with specific primary antibodies. After extensive washings and incubation for 1 h at room temperature with secondary antibodies conjugated with horseradish peroxidase (Amersham Biosciences), immunoreactivity was analyzed by means of the chemiluminescence detection system (ECL, Amersham Biosciences).

GST Fusion Protein Expression—GST fusion proteins expression was induced in *Escherichia coli* BL21 cells with 0.1–1.0 mM isopropyl-1-thio-β-D-galactopyranoside for 3 h. Cells were harvested by centrifugation, and after sonication on ice, the lysates were incubated 10 min at 4 °C with the glutathione-Sepharose 4B beads (Amersham Biosciences).

GST Pulldown Assay—Solubilized proteins from skeletal muscle microsomes or from cell lysates were precleared 30 min at 4 °C with glutathione-Sepharose 4B beads. 500 μg of each lysate were incubated with 15 μg of fusion protein (50 μl of beads, 50% slurry) for 2 h at 4 °C in a pulldown buffer (20 mM Tris, pH 8, 200 mM NaCl, 1% Triton X-100, 1 mM PMSF, 1 mM Na_3VO_4, 1 mM EDTA, pH 8, and protease inhibitors), and then the complexes were washed four times with 0.1% SDS pulldown buffer. Bound proteins were eluted and subjected to SDS-PAGE and immunoblot analysis as described previously.

Antibodies—The antibodies used in the experiments were: anti-caveolin-3 (mouse, BD Biosciences); A1 monoclonal anti-α1s-DHPR (Thermo Scientific); anti-α1s-DHPR (sheep), kindly provided by Dr. K. Campbell; anti-RyR (34C, mouse, Thermo Scientific); anti-RyR1 (R-162, rabbit, Ref. 29); anti-JP1 (rabbit, Zymed Laboratories Inc.); anti-JP2 (rabbit, Zymed Laboratories Inc.; goat, Santa Cruz Biotechnology). For immunofluorescence experiments, the Cy3-conjugated secondary antibodies against goat, mouse, and rabbit were purchased from Jackson ImmunoResearch Laboratories; for immunoblot experiments, the HRP-conjugated secondary antibodies against mouse, rabbit, and sheep were purchased from Amersham Biosciences.

Plasmids—To produce recombinant GST fusion proteins, specific sequence covering different cytosol-specific regions of human JP1 and JP2 were cloned in the pGEX-4T1 (GE-Healthcare) vector obtaining GST-JP1A (aa 1–231), GST-JP1B (aa 232–369), GST-JP1C (aa 369–571), GST-JP2A (aa 1–253), GST-JP2B (aa 216–399), and GST-JP2C (aa 379–594) plasmids. Gene silencing was performed by cloning sequences targeting JP1 and JP2 murine mRNA in pSuper vector (Oligoengine).

Electrophysiology and Confocal Ca^{2+} Imaging in Voltage-clamped C2C12 Myotubes—Ca^{2+} current and intramembrane charge movement measurements in C2C12 myotubes were performed with the standard whole-cell configuration of the patch clamp technique using an RK400 patch clamp amplifier (Bio-Logic, Claix, France). Command voltage pulse generation and data acquisition were done using the pClamp10 software (Axon Instruments Inc., Downingtown, PA) driving an A/D converter (Digidata 1322A, Axon Instruments Inc.). Voltage clamp was performed with a pipette filled with a solution containing 10 mM EGTA (see "Solutions"). Holding potential was set to −80 mV. The voltage dependence of the peak Ca^{2+} current density was fitted with the following equation

$$I(V) = G_{max}(V - V_{rev})/[1 + \exp[(V_{0.5} - V)/k] \quad \text{(Eq. 1)}$$

with $I(V)$ being the peak current density at the command potential V, G_{max} being the maximum conductance, V_{rev} being the reversal potential, $V_{0.5}$ being the half-activation potential, and k being a steepness factor. Intramembrane charge movement was measured in response to 25 ms-long depolarizing test pulses of increasing amplitude applied for 50 ms following a 1-s-long pulse from −80 to −20 mV, to minimize the contribution of Na^+ and T-type Ca^{2+} channels (32). Charge movement currents were analyzed according to previously described procedures (33, 34). Confocal imaging of rhod-2 Ca^{2+} transients was done in separate experiments using a Zeiss LSM 5 laser scanning confocal microscope equipped with a ×63 oil immersion objective (N.A. 1.4). For detection of GFP fluorescence, the excitation was provided by the 488 nm line of an argon laser, and a 505 nm long pass filter was used on the detection channel. For measurements of rhod-2 fluorescence, the excitation was from the 543 nm line of a HeNe laser, and fluorescence was collected above 560 nm. The pinhole aperture was usually set to 1 airy unit, although in a few experiments, a larger value was used. Voltage clamp was achieved as described above except that the pipette solution contained 0.2 mM EGTA and 100 μM rhod-2. Command voltage pulse generation was achieved using identical equipment as used for the Ca^{2+} current measurements. Intracellular [Ca^{2+}]-related rhod-2 fluorescence changes were imaged using the line-scan mode of the system, synchronized with the voltage pulse generation. Line-scan images (512/2,048 pixels) were taken with a time resolution of 1.15 ms/line. Image processing and analysis were performed using ImageJ (National Institutes of Health) and MicroCal Origin (OriginLab, Northampton, MA). Care was taken that the analysis excluded portions of the line that went across nuclei. Changes in rhod-2 fluorescence were expressed as F/F_0 where F_0 is the resting (or baseline) fluorescence level.

Solutions—For Ca^{2+} current measurements in cultured myotubes, the pipette solution contained (in mM): 110 cesium aspartate, 20 TEA-Cl, 2 $MgCl_2$, 5 Mg-ATP, 10 EGTA, and 10 HEPES, and the extracellular solution contained (in mM) 140 TEA-methanesulfonate, 10 $CaCl_2$, 2 $MgCl_2$, 0.001 TTX, and 10

HEPES. For intramembrane charge movement measurements, the pipette solution contained (in mM): 110 cesium aspartate, 20 TEA-Cl, 5 $MgCl_2$, 10 EGTA, and 10 HEPES, and the extracellular solution contained (in mM) 140 TEA-methanesulfonate, 10 $CaCl_2$, 2 $MgCl_2$, 0.5 $CdCl_2$, 0.3 $LaCl_3$, 0.003 TTX, and 10 HEPES. For Ca^{2+} transient measurements, the pipette solution contained (in mM): 110 cesium aspartate, 20 TEA-Cl, 2 $MgCl_2$, 5 Mg-ATP, 5 Na_2-phosphocreatine, 0.2 EGTA, 0.1 rhod-2, and 10 HEPES, and the extracellular solution contained (in mM) 140 TEA-methanesulfonate, 2.5 $CaCl_2$, 2 $MgCl_2$, 0.002 TTX, and 10 HEPES. The pH of all solutions was adjusted to 7.20. For Ca^{2+} current measurements in adult fibers, the pipette solution contained (in mM): 120 potassium glutamate, 5 Na_2-ATP, 5 Na_2-phosphocreatine, 5.5 $MgCl_2$, 5 glucose, 10 EGTA, and 5 HEPES, and the extracellular solution contained (in mM) 140 TEA-methanesulfonate, 2.5 $CaCl_2$, 2 $MgCl_2$, 0.002 TTX, 1 4-aminopyridine, and 10 HEPES. For Ca^{2+} transient measurements in adult fibers, the pipette solution was of identical composition except that it also contained (in mM) 4 $CaCl_2$ and 0.2 rhod-2. The extracellular solution used for Ca^{2+} transient measurements in adult fibers contained (in mM) 140 TEA-methanesulfonate, 2.5 $CaCl_2$, 2 $MgCl_2$, 0.002 TTX, and 10 HEPES. The pH of all solutions was adjusted to 7.20.

Statistics—Least-squares fits were performed using a Marquardt-Levenberg algorithm routine included in MicroCal Origin (OriginLab). Data values are presented as mean ± S.E. for n fibers tested. Statistical significance was determined using Student's t test assuming significance for $p < 0.05$.

Transfection of Adult Interosseus Muscles and Preparation of Isolated Fibers—Experiments were performed using 8-week-old male OF1 mice (Charles River Laboratories, L'Arbresle, France). The electroporation protocol and procedures for enzymatic isolation of single fibers and partial insulation of the fibers with silicone grease were as described previously (35, 36). All experiments and procedures were performed in accordance with the guidelines of the local animal ethics committees of the University Lyon 1 and University of Siena.

Electrophysiology and Confocal Ca^{2+} Imaging in Voltage-clamped Adult Muscle Fibers—Ca^{2+} current measurements in adult muscle fibers were performed with the silicone voltage clamp technique using an RK400 patch clamp amplifier (35). Voltage clamp was performed as described above for the Ca^{2+} current measurements in adult fibers except that the pipette was filled with a solution containing 10 mM EGTA, 4 mM $CaCl_2$ and 0.2 mM rhod-2 (see "Solutions"). Changes in $[Ca^{2+}]$ were calculated from the F/F_0 rhod-2 signals using the previously described pseudo-ratio Equation 1 assuming a basal $[Ca^{2+}]$ of 100 nM and a K_d of rhod-2 for Ca^{2+} of 1.2 μM. An estimation of the Ca^{2+} release flux underlying the thus calculated global $[Ca^{2+}]$ transients was performed according to a previously described procedure (34–36).

RESULTS

Molecular Interaction between Junctophilin 1 and 2 and the α1s Subunit of the DHPR—Starting from the evidence that JP1 interacts with the RyR1 on the SR, we wanted to verify whether JPs may also interact with proteins on the T-tubule/plasma membrane, like the α1s subunit of the DHPR. Analysis by

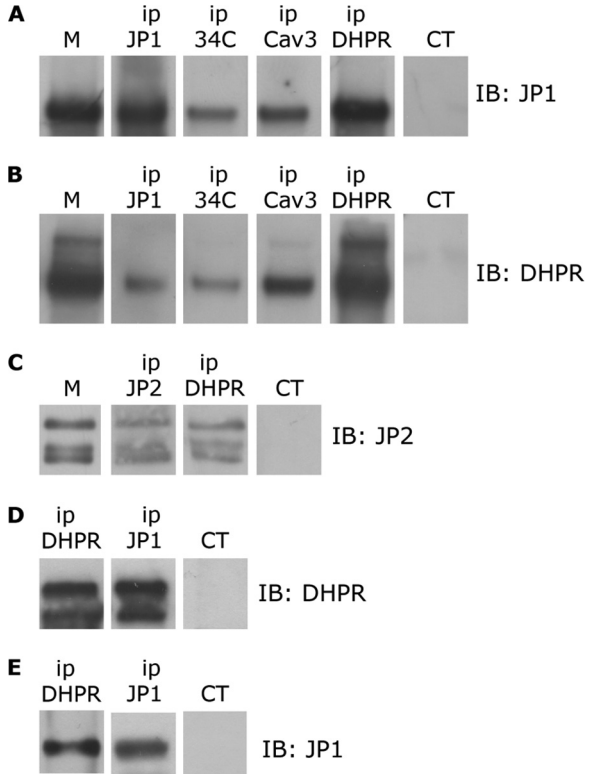

FIGURE 1. **Immunoprecipitation of DHPR, JP1, and JP2 from solubilized rabbit skeletal muscle and HEK293-T microsomes.** *A*, 100 μg of proteins solubilized from rabbit skeletal muscle microsomes (*M*) were immunoprecipitated (*ip*) with antibodies against JP1, RyR (*34C*), caveolin-3 (*Cav3*), α1s-DHPR (*DHPR*), and a non-correlated control antibody (*CT*). After gel electrophoresis, proteins were transferred to a nylon membrane and incubated with anti-JP1 antibody. *B*, 100 μg of proteins solubilized from skeletal muscle microsomes were immunoprecipitated with antibodies against JP1, RyR, caveolin-3, and α1s-DHPR and a non-correlated control antibody. After gel electrophoresis, proteins were transferred to a nylon membrane and incubated with an antibody against α1s-DHPR. *C*, 100 μg of proteins solubilized from rabbit skeletal muscle microsomes were immunoprecipitated with antibodies against JP2, α1s-DHPR, and a non-correlated control antibody. After gel electrophoresis, proteins were transferred to a nylon membrane and incubated with anti-JP2 antibody. *D*, solubilized proteins from HEK293-T cells transfected with pEGFP-α1s-DHPR, pEGFP-β1a-DHPR, and pCDNA-JP1 were immunoprecipitated with antibodies against α1s-DHPR, JP1, and a non-correlated control antibody. Proteins were separated by gel electrophoresis, transferred to a nylon membrane, and incubated with an antibody against DHPR. *E*, solubilized proteins from HEK293-T cells transfected with pEGFP-α1s-DHPR, pEGFP-β1a-DHPR, and pCDNA-JP1 were immunoprecipitated with antibodies against α1s-DHPR, JP1, and a non-correlated control antibody. Proteins were separated by gel electrophoresis, transferred to a nylon membrane, and incubated with an anti-JP1 antibody.

Western blot and immunoprecipitation of proteins solubilized from skeletal muscle microsomes with an anti-JP1 antibody revealed a band at 90 kDa, as shown in Fig. 1. Identical results were obtained with two different antibodies (data not shown), confirming the identity of the observed 90-kDa protein as JP1 (10, 19). Interestingly, JP1 was immunoprecipitated by an antibody against caveolin 3 (Cav3) and by an antibody directed against the α1s subunit of the DHPR (Fig. 1*A*). No specific band was observed when an unrelated antibody was used (Fig. 1, *A* and *B*). These results were confirmed by paired experiments where we observed that the α1s subunit of DHPR was immunoprecipitated with antibodies against JP1 and Cav3 (Fig. 1*B*). In agreement with published results, we confirmed that JP1 was also immunoprecipitated with the antibody 34C against RyR1

(19, 20). Interestingly, we observed that the antibody 34C against RyR1 also immunoprecipitated the α1s subunit of DHPR (Fig. 1*B*). Co-immunoprecipitation of RyR1 and DHPR has been previously reported by Marty and colleagues (37–39). Although supported by many physiological data, this co-immunoprecipitation has been often difficult to be directly demonstrated (40, 41). Altogether, these results indicate that JP1 is part of a complex made up by RyR1, DHPR, and Cav3. Because skeletal muscles, in addition to JP1, also express JP2, we wanted to verify whether JP2 might also associate with the complex of proteins immunoprecipitated with the DHPR. Western blot analysis and immunoprecipitation of proteins solubilized from skeletal muscle microsomes with an antibody against JP2 revealed a JP2-specific band of about 100 kDa, plus two additional bands, likely degradation product (Fig. 1*C*). A superimposable staining was also observed using a second distinct antibody against JP2, confirming the specificity of the observed signal as JP2 (data not shown). In addition, JP2 was also immunoprecipitated with an antibody against the α1s subunit of DHPR (Fig. 1*C*).

To confirm the interaction between JP1 and DHPR and to examine whether the association between JP1 and the α1s subunit of the DHPR may require other muscle-specific proteins, we performed a similar set of immunoprecipitation experiments in HEK293-T cells transfected with plasmids encoding pEGFP-α1s-DHPR, pEGFP-β1a-DHPR, and pCDNA-JP1. 100 μg of proteins solubilized from transfected cells were immunoprecipitated with antibodies directed against JP1 as well as with antibodies directed against the α1s subunit of DHPR. Immunocomplexes were separated by SDS-PAGE and analyzed by Western blot. As shown in Fig. 1*D*, the α1s subunit of DHPR was immunoprecipitated with an antibody against the α1s subunit of DHPR and with an anti-JP1 antibody, but was absent in samples incubated with an unrelated antibody. The interaction between the α1s subunit of the DHPR and JP1 was also confirmed in immunoprecipitation experiments performed with antibody directed against the α1s subunit of DHPR followed by Western blot with antibody against JP1 (Fig. 1*E*). These results, in addition to confirm the association between the two proteins, demonstrate that the interaction between JP1 and DHPR does not require other muscle-specific proteins. Similar experiments aimed at verifying a direct interaction between JP2 and α1s subunit of the DHPR in HEK293-T cells did not yield reproducible results, indicating either that JP2 does not directly interact with the α1s subunit of the DHPR or that this interaction is too weak to be reproduced *in vitro*.

Identification of a Region on JP1 and JP2 Enabling the Interaction with α1s Subunit of the DHPR—To determine the region of JP1 involved in binding to the α1s subunit of the DHPR, we prepared recombinant GST fusion proteins in the pGEX-4T1 vector that cover different cytosol-specific regions of JP1, indicated as GST-JP1A (aa 1–231), GST-JP1B (aa 232–369), and GST-JP1C (aa 369–571). For GST pulldown experiments, 10 μg of purified GST and GST-JP1 or GST-JP2 fusion proteins, immobilized on glutathione-Sepharose 4B affinity beads, were incubated for 2 h at 4 °C with 500 μg of proteins from solubilized microsomes from skeletal muscle. To avoid nonspecific binding, solubilized microsomal proteins were first precleared

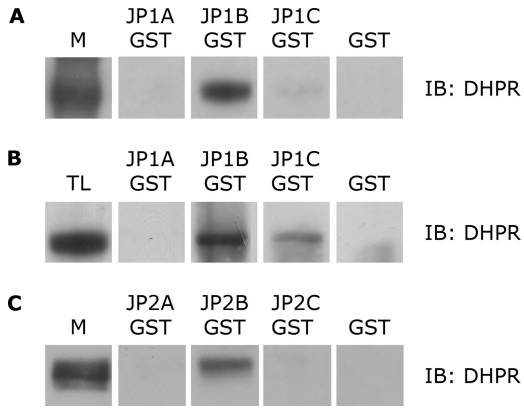

FIGURE 2. **Association of DHPR with JP1-B in skeletal muscle and in HEK293-T transfected cells.** *A*, Western blot (*IB*) with an anti-α1s-DHPR antibody of solubilized rabbit skeletal muscle microsomes (*M*) and of proteins pulled down with GST-JP1-A, GST-JP1-B, GST-JP1-C, and GST alone, as negative control. *DHPR*, anti-α1s-DHPR antibody. *B*, Western blot with an anti-α1s-DHPR antibody of lysates of HEK293-T cells transfected with pEGFP-α1s-DHPR, pEGFP-β1a-DHPR, and pCDNA-JP1 (*TL*) and of proteins pulled down with GST-JP1-A, GST-JP1-B, GST-JP1-C, and GST alone, as negative control. *C*, Western blot with an anti-α1s-DHPR antibody of solubilized rabbit skeletal muscle microsomes and proteins pulled down with GST-JP2-A, GST-JP2-B, GST-JP2-C, and GST alone, as negative control.

with glutathione-Sepharose beads at 4 °C. As shown in Fig. 2*A*, Western blot analysis with an antibody against the α1s subunit of DHPR revealed that GST-JP1B fusion protein and, at a much lower degree, GST-JP1C were able to pull down the endogenous α1s subunit of the DHPR, whereas GST-JP1A and GST peptide alone did not appear to bind the α1s subunit of the DHPR. Pulldown assays were repeated with cell lysates from HEK293-T cells transfected with pEGFP-α1s-DHPR and pEGFP-β1a-DHPR. As shown in Fig. 2*B*, GST-JP1B and, at a lower degree, GST-JP1C, but not GST-JP1A or GST alone, were able to bind the α1s subunit of the DHPR. Altogether, these results showed that in addition to RyR1, JP1 also associates with the α1s subunit of the DHPR through a sequence included between amino acids 232 and 369. The weaker signal obtained with the GST-JP1-C construct that comprises amino acids 369–571 of JP1 may suggest that the binding site could comprise a wider region that includes part of JP1-C.

To test the interaction between specific regions of JP2 and the α1s subunit of the DHPR, specific sequences covering different cytosolic specific regions of JP2 were cloned in the pGEX-4T1 vector to obtain recombinant GST fusion proteins indicated as GST-JP2A (aa 1–253), GST-JP2B (aa 216–399), and GST-JP2C (aa 379–594). Western blot analysis with antibody against the α1s subunit of DHPR revealed that the GST-JP2B fusion protein was able to pull down the endogenous α1s subunit of the DHPR from solubilized microsomal proteins prepared from skeletal muscle, whereas GST-JP2A, GST-JP2C, and GST alone did not (Fig. 2*C*). Altogether, these experiments suggested that the interaction between JP2 and the α1s subunit of the DHPR is mediated by a region superimposable to the one observed with JP1. Parallel pulldown experiments, using GST-JP2 fusion proteins and lysates from HEK293-T cells transfected with pEGFP-α1s-DHPR and pEGFP-β1a-DHPR, did not yield reproducible results.

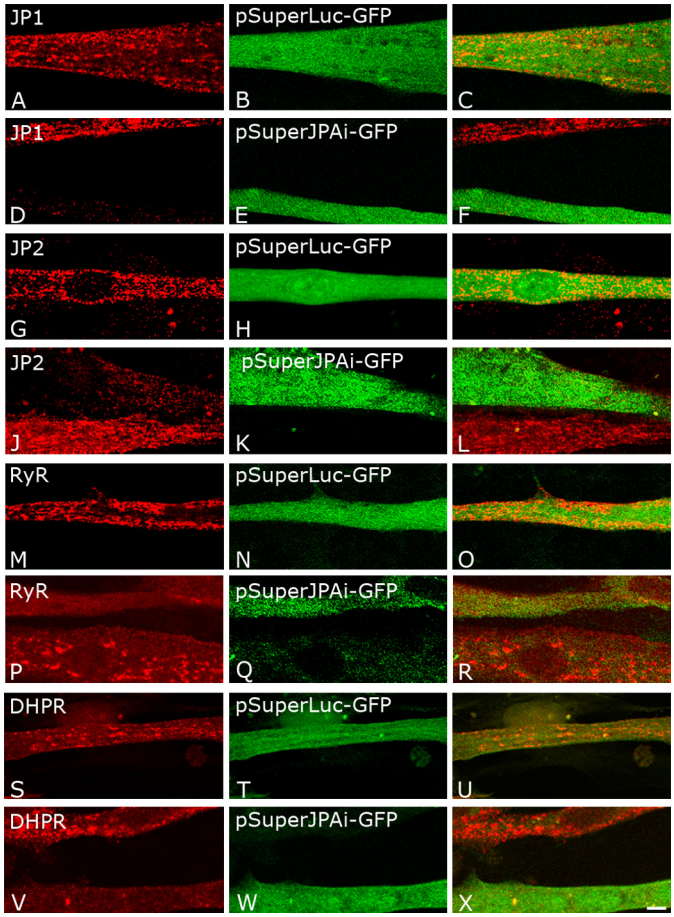

FIGURE 3. **Immunofluorescence analysis of expression inhibition of JP1 and JP2 in C2C12 cells.** C2C12 cells were transfected with pSuperLuc-GFP as negative control (*A–C*, *G–I*, *M–O*, and *S–U*) or with pSuperJPAi-GFP to silence JP1 and JP2 expression (*D-F*, *J–L*, *P–R*, and *V–X*). C2C12 cells transfected with pSuperLuc-GFP were immunostained with antibodies against JP1 (*A–C*), JP2 (*G–I*), RyR (*M–O*), and α1s DHPR (*S–U*). C2C12 cells were transfected with pSuperJPAi-GFP were immunostained with antibodies against JP1 (*D–F*), JP2 (*J–L*), RyR (*P–R*), and α1s-DHPR (*V–X*).

Knockdown of JP1 and JP2 Alters the Punctate Pattern of RyR and DHPR in Cultured C2C12 Myotubes—Because the results obtained from immunoprecipitation and pulldown experiments strongly indicated that JP1 and JP2 could interact with the α1s subunit of the DHPR on the T-tubule membrane as well as with the RyR Ca^{2+} release channel on the sarcoplasmic reticulum, we wanted to verify the effect of JP1 and JP2 ablation in C2C12 by transfecting plasmids capable of expressing an siRNA specifically targeted against these two JP isoforms. In preliminary experiments, we tested different vectors expressing different siRNAs targeting either JP1 or JP2, including one siRNA (JPAi) that had been previously reported to affect the expression of both JP isoforms (26). Indeed, expression of the pSuperJPAi-GFP vector, which identifies a common sequence in JP1 and JP2, consistently resulted in a strong reduction in the intensity of both JP1 and JP2 signals in transfected cells (Fig. 3, *D* and *J*). Because we could not obtain a high frequency of transfection, to test the effect of different siRNA-expressing vectors, we decided to quantify the intensity of the fluorescence signal obtained with antibodies against either JP1 and JP2 in cells transfected with the siRNA-expressing vectors against neighbor cells. Analysis of the mean fluorescence signal of JP1 and JP2 in cells expressing the pSuperJPAi-GFP siRNA revealed a reduction of 66 ± 13 and to 59 ± 18% in 21 and 24 cells, respectively ($p < 0{,}001$) when compared with untransfected cells (Fig. 3, *D–F* and *J–L*). In cells expressing a nonrelevant control siRNA (pSuperLuc-GFP), JP1 and JP2 signals were not significantly altered (Fig. 3, *A–C* and *G–I*). C2C12 myotubes transfected with pSuperJPAi-GFP and pSuperLuc-GFP were then stained with antibodies specific to the α1s subunit of the DHPR and RyR. Staining for the α1s subunit of the DHPR and RyR of myotubes transfected with the pSuperLuc-GFP expressing the unrelated control siRNA consistently yielded a punctated pattern (Fig. 3, *M–O* and *S–U*) similar to that observed in untransfected C2C12 cells. In striking contrast and in a highly reproducible manner, in C2C12 myotubes transfected with the pSuperJPAi-GFP vector, the DHPR and the RyR signals did not present the punctated pattern typical of triadic proteins, but the fluorescence signal was rather diffuse. To better evaluate this point, the size of puncta was analyzed by the ImageJ software in control and knocked down C2C12 cells. Puncta were sorted depending on their area, where a limit of 0.163 μm^2 was fixed to subdivide puncta into small (< 0.163 μm^2) and large (>0.163 μm^2) puncta. According to this analysis, the frequency of well defined large puncta in C2C12 cells transfected with the control pSuperLuc-GFP plasmid was 19% ± 7.9, whereas in C2C12 cells knocked down for JP1 and JP2, it was 9.3% ± 5.8 ($p < 0.05$). (See also Fig. 3, P–R and *V–X* for representative images.)

Furthermore, the fluorescence signal obtained following staining with the antibody against the α1s subunit of the DHPR in myotubes transfected with the pSuperJPAi-GFP vector was consistently dimmer than that observed in control cells. When calculated, the mean immunofluorescence signal of the α1s subunit of the DHPR in cells expressing the pSuperJPAi-GFP siRNA was reduced 37 ± 15% in 18 cells, $p < 0{,}001$. The reduction in the intensity of the fluorescent signal observed in myotubes transfected with pSuperJPAi-GFP vector was specific for the DHPR as it was not observed when cells were stained with antibody against RyR (10 ± 20% in 22 cells). No consequence on the pattern or the levels of expression of RyR and DHPR signals was observed in cells transfected with pSuper-GFP vectors targeting selectively either JP1 or JP2 (data not shown), suggesting the contribution of both JPs to the organization of these junctional proteins. No effect was observed in the intensity of the DHPR and RyR fluorescence signals in cells transfected with the control pSuperLuc-GFP.

Knockdown of JPs in Cultured Myotubes Depresses the Functional Activity of the DHPR without Affecting Ca^{2+} Release—Fig. 4*A* shows illustrative records of the voltage-activated Ca^{2+} current from a control (*left*) and from a pSuperJPAi-GFP-positive (*right*) myotube. The current was measured in response to pulses from −80 mV to values ranging between −10 and +30 mV with a 10-mV increment. Fig. 4*B* shows the mean voltage dependence of the peak current and of the corresponding conductance from five control and six pSuperJPAi-GFP-positive myotubes. There was a dramatic reduction of the L-type Ca^{2+} current density, corresponding to an ~50% reduction of the peak conductance. Fitting the voltage dependence of the peak

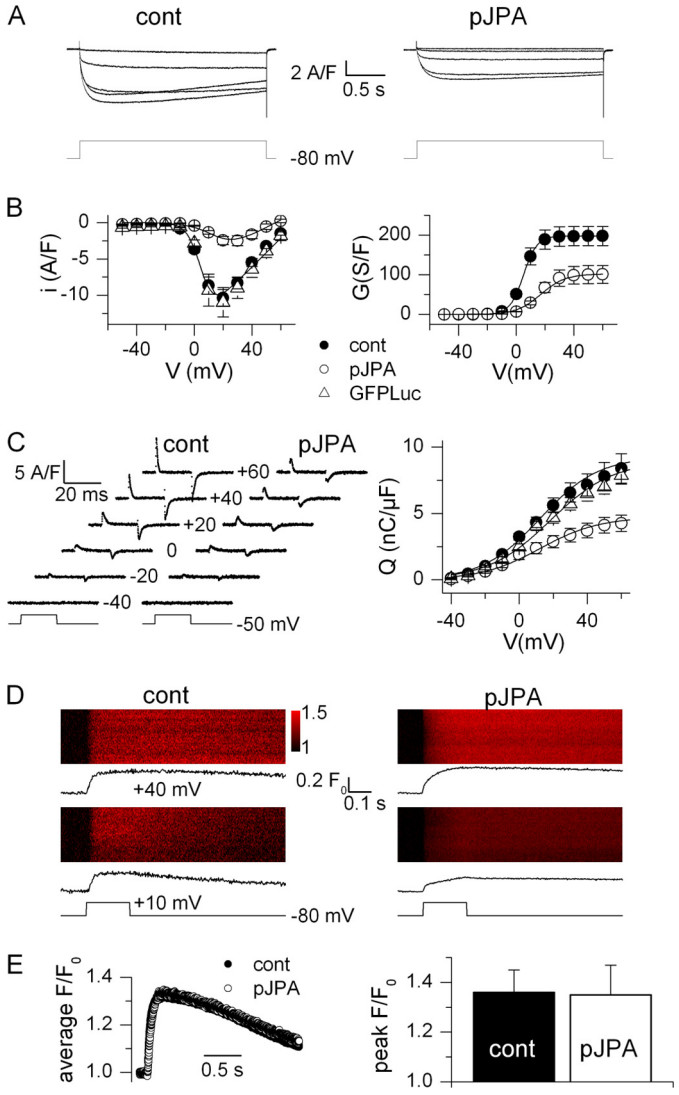

FIGURE 4. **DHPR-mediated Ca^{2+} entry, charge movement, and Ca^{2+} release in control and JP knockdown C2C12 myotubes.** *A*, Ca^{2+} current traces obtained in a control myotube (*cont*, *left*) and in a pSuperJPAi-GFP-positive myotube (*pJPA*, *right*) in response to the depolarizing pulse protocol illustrated below. *B*, mean voltage dependence of the peak Ca^{2+} current density (*left*) and corresponding mean maximum conductance (*right*) in control ($n = 5$), pSuperJPAi-GFP-positive ($n = 6$), and pSuperLuc-GFP-positive ($n = 5$) myotubes. *Superimposed lines* were calculated from the average values of the parameters obtained from fitting the appropriate function to the individual series of data (see "Experimental Procedures"). *C*, *left*, charge movement currents measured in a control and in a pSuperJPAi-GFP-positive myotube at the indicated values of membrane potential. *Right*, mean voltage dependence of charge density in control ($n = 13$), pSuperJPAi-GFP-positive ($n = 9$), and pSuperLuc-GFP-positive myotubes ($n = 10$). *Superimposed lines* were calculated from the average values of the parameters obtained from fitting a Boltzmann function to the individual series of data. *D*, line-scan images of the rhod-2 fluorescence taken from a control myotube (*left*) and from a pSuperJPAi-GFP-positive myotube (*right*). Vertical size corresponds to 100 μm. Myotubes were stimulated by a 200-ms-long voltage clamp depolarization from −80 mV to the indicated level. The average time course of change in rhod-2 fluorescence is shown underneath each line-scan image. *E*, *left*, average rhod-2 fluorescence transient elicited by a depolarizing pulse to +40 mV in nine control and seven pSuperJPAi-GFP-positive myotubes. *Right*, corresponding mean (± S.E.) peak amplitude of the rhod-2 transient in the two sets of myotubes.

current in each cell gave mean values for G_{max}, V_{rev}, $V_{0.5}$, and k of 198 ± 24 s/F, 70.9 ± 1.5 mV, 5.0 ± 0.9 mV, and 4.8 ± 0.2 mV in control myotubes and of 102 ± 22 s/F, 56.4 ± 3.4 mV, 17.2 ± 2.8 mV, and 8.5 ± 3.1 mV in pSuperJPAi-GFP-positive myotubes, respectively. The peak conductance value was significantly depressed in the pSuperJPAi-GFP-positive cells ($p = 0.016$), the reversal potential was reduced ($p = 0.006$), and the voltage for half-activation was right-shifted ($p = 0.004$). The reduction of the reversal potential was likely to result from the very low amplitude of the Ca^{2+} current that unmasked residual outward K^+ conductances. A series of measurements was also made in myotubes transfected with the pSuperLuc-GFP plasmid, used as a negative control; mean values for the peak current density from five pSuperLuc-GFP-positive cells are shown in Fig. 4*B*. Corresponding values for G_{max}, V_{rev}, $V_{0.5}$, and k were 187 ± 13 s/F, 70 ± 3.2 mV, 6.8 ± 1.1 mV, and 5.1 ± 0.5 mV, not statistically different from the control values. The presence of the JP proteins thus appears to be an important determinant of the proper Ca^{2+} channel function of the DHPR.

Fig. 4*C* shows intramembrane charge movement current traces (*left*) from a control and from a pSuperJPAi-GFP-positive myotube and the mean distribution of charge *versus* membrane voltage (*right*) in the three groups of myotubes. Knockdown of JPs was associated with a reduction of intramembrane charge movement; fitting a two-state Boltzmann distribution in each cell gave mean values for Q_{max} of 9.3 ± 3 ($n = 13$), 4.7 ± 0.7 ($n = 9$), and 9.0 ± 0.7 nanocoulombs/μF ($n = 10$) in control and pSuperJPAi-GFP-positive myotubes, respectively. Mean values for the voltage of equal charge distribution and for the steepness factor did not differ between the three groups. These results indicate an ~50% reduction of both the voltage-sensing and the Ca^{2+} channel functions of the DHPR, most likely to result from a loss of DHPR protein in the plasma membrane, in accordance with the immunostaining data.

Because the DHPR controls the opening and closing of the ryanodine receptor during e-c coupling, a functional alteration of this process under the conditions of JP knockdown was anticipated. Whole-cell voltage clamp-activated Ca^{2+} transients were measured in control and pSuperJPAi-GFP-positive myotubes using the Ca^{2+} indicator rhod-2 (supplemental Fig. S1).

Fig. 4*D* shows line-scan images of the rhod-2 fluorescence taken from a control myotube (*left*) and from a pSuperJPAi-GFP-positive myotube (*right*) while applying a 0.2-s-long depolarizing pulse to the cell. The corresponding F/F_0 signal is shown underneath each image. The line-scan images from the pSuperJPAi-GFP-positive myotube clearly show that knockdown of JPs did not preclude SR Ca^{2+} release in response to the depolarizing pulses. Fig. 4*E* shows the average time course of the rhod-2 fluorescence transient elicited by a depolarizing pulse to +40 mV in nine control and seven pSuperJPAi-GFP-positive myotubes (left) and the corresponding mean peak amplitude (± S.E.) of the transient. There was no indication of any substantial alteration of SR Ca^{2+} release due to the loss of JPs.

Of specific relevance was also the possibility to question the consequences of JP underexpression in a fully differentiated muscle preparation where the triadic architecture and molecular interactions of the e-c coupling partners are optimally organized. For this, we used *in vivo* transfection of the same cDNA construct in adult mouse muscle fibers (31). Results showed that there was a slight reduction of the L-type Ca^{2+} current density, corresponding to an ~25% reduction of the peak con-

ductance (supplemental Fig. S2, *A* and *B*). Interestingly the activation and inactivation kinetics of the Ca^{2+} current were also slower in the pSuperJPAi-GFP-positive fibers than in the control ones. For instance, the mean value for the time to peak of the Ca^{2+} current at +20 mV was 143 ± 13 ms ($n = 9$) and 94 ± 5 ms ($n = 13$) in control and pSuperJPAi-GFP-positive fibers, respectively; the time constant of Ca^{2+} current decay was 222 ± 53 ms ($n = 13$) at +20 mV in control fibers, whereas in nine pSuperJPAi-GFP-positive fibers, the decay was much too slow to be reliably fitted by a single exponential. This is clearly indicating that functional properties of the DHPR Ca^{2+} channels are altered in adult fibers in situation of JP deficiency. However, as in the cultured myotubes, we found no corresponding effect on voltage-activated Ca^{2+} release supplemental Fig. S2, *C* and *D*).

DISCUSSION

JP1 and JP2 have a key role in anchoring the SR to the T-tubule/sarcolemma membrane in striated muscles, thus contributing to the formation and stabilization of specialized junctional membrane complexes where proteins that participate in the mechanism of e-c coupling are localized. Additional evidence suggests that JPs might also participate in the regulation of Ca^{2+} homeostasis. This appears to occur either via direct protein-protein interaction between JPs and SR and sarcolemma proteins such as RyR and TRPC3 channels (18, 20, 21, 26) or indirectly as proposed for STIM1-Orai1-dependent mechanisms of Ca^{2+} entry at the plasma membrane (23). Our present results further establish this overlapping function in Ca^{2+} signaling by uncovering interactions between JP1 and JP2 with the DHPR, making JPs now also involved in the regulation of voltage-gated Ca^{2+} entry in skeletal muscle cells. The association between the JP1 and JP2 and DHPR was observed in co-immunoprecipitation and pulldown experiments with solubilized proteins from skeletal muscle microsomes. The same experiments indicated that RyR1 and Cav3 are also part of the protein complex that was immunoprecipitated together with JP1 and DHPR. The interaction with the DHPR was mapped to a sequence between aa 232–369 of JP1 and the corresponding region in JP2. The interaction between DHPR and JP1, but not with JP2, was further confirmed in HEK293-T cells expressing heterologous proteins, indicating that DHPR and JP1 may interact directly. Altogether, our results suggest that JP1 and JP2 are part of a complex made up by at least two other proteins crucial for e-c coupling, DHPR and RyR.

The significance of these interactions is further extended by results obtained in immunofluorescence experiments in C2C12 cells following knockdown of JPs, where the staining for DHPR and RyR was not present with the typical punctated pattern usually observed for junctional proteins. Indeed, following JP knockdown, the immunofluorescence signals for DHPR and RyR appeared more diffused and less organized in clusters than in control cells. Reduced clustering of RyR and DHPR in C2C12 after knockdown of JPs might result from the reduction in junctional membrane complexes due to reduced levels of JPs (7, 18). However, it might also indicate that retention of RyR and DHPR within the junctional membrane complexes may be dependent, at least in part, on interactions with JPs. It is worth noticing that no alteration in the immunofluorescence patterns of RyR and DHPR was ever observed when pSuper-GFP vectors expressing siRNAs selective for either JP1 or JP2 were used separately (data not shown), suggesting that to modify the clustering of RyR and DHPR from larger puncta into a more diffused pattern in differentiated C2C12 cells, a reduced expression of both JP1 and JP2 is required. In addition, we noted that in JP knockdown cells, the DHPR signal, but not that of RyR, was reduced. The effects of JP depletion on DHPR were further confirmed by results from experiments performed under voltage clamp conditions, where knockdown of JPs was associated with a reduction of L-type Ca^{2+} current and of intramembrane charge movement. The Ca^{2+} current was also found reduced in adult muscle fibers, although to a smaller extent than in the cultured myotubes, likely due to the less effective depression of JPs in the myofibers *in vivo*. Altogether, these results are consistent with a drop of DHPR protein density in the sarcolemma, indicating that either the decreased availability of junctional membrane complex and/or the reduced interactions with JPs lowered the expression of DHPRs, but not of RyRs, in JP knockdown muscle cells. This could reflect a specific requirement of the DHPR for JP expression when compared with RyR. Actually, one unexpected finding of our study was the lack of concomitant major alteration of voltage-activated Ca^{2+} release; indeed, this tends to not only exclude a decisive role of JPs in the acute control of RyR1 channels but also suggests that a 35–50% (from our immunostaining and charge movement data) reduction in DHPR molecules still leaves the system with a sufficient amount of voltage sensors to secure the function of e-c coupling. This obviously is puzzling, and there is to our knowledge no previously reported experimental situation where such straight dissociation between DHPR density and SR Ca^{2+} release was observed. Rather, a number of studies reported parallel changes in DHPRs and Ca^{2+} release, as for instance in aging muscle (42). Still, in the simplest framework, activation of SR Ca^{2+} release is pictured to operate through voltage-dependent recruitment of a homogeneous population of DHPR tetrads, each contributing to activate an identical fraction of the RyR1 channels. Present results would suggest that there might be redundancy in the system so that a substantial fraction of DHPRs can be lost without necessarily compromising the Ca^{2+} release capability of the cell. Although this may appear as a subversive hypothesis, it would actually offer an additional safety mechanism for the control of muscle contraction. An alternative would be to consider that functional consequences of JP knockdown included an increased effectiveness of voltage sensor charge movements to activate RyR channels or that under these experimental conditions, a Ca^{2+}-induced Ca^{2+} release-like mechanism might help to ensure full activation of SR Ca^{2+} release. The absence of an alteration of voltage-activated SR Ca^{2+} release observed here does not preclude the possibility that, under either intense or prolonged periods of activity, proper maintenance of intracellular Ca^{2+} regulation and e-c coupling may be affected by the reduced DHPR function. Along this line, data from Hirata *et al.* (26) showed that JP-deficient muscle fibers stimulated repetitively in the absence of extracellular Ca^{2+} failed to develop Ca^{2+} transients more rapidly than control muscle fibers. Although the authors favored a

role of defective store-operated calcium entry mechanism, the possible contribution of reduced DHPR activity may be speculated to also contribute to this type of effect.

In conclusion, based on the above reported findings, we propose that JP1 and JP2, in addition to their role in the formation of structural junctional membrane complexes between the SR and T-tubule/sarcolemma, can also provide a scaffold-like function that might help in establishing functional interactions between junctional proteins, including DHPR and RyRs, and thus further help in the establishment of the mechanism of e-c coupling.

Acknowledgments—We thank Manfred Grabner for providing pEGFP-α1s-DHPR and pEGFP-β1a-DHPR plasmids and Hiroshi Takeshima for providing the junctophilin 2 plasmid.

REFERENCES

1. Franzini-Armstrong, C. (2004) in *Myology* (Engel, A. G., and Franzini-Armstrong, C., eds) pp. 232–256, McGraw-Hill, Inc., New York, NY
2. Sorrentino, V. (2011) *Int. J Biochem. Cell Biol.* **43,** 1075–1078
3. Rossi, A. E., and Dirksen, R. T. (2006) *Muscle Nerve* **33,** 715–731
4. Takahashi, M., Seagar, M. J., Jones, J. F., Reber, B. F., and Catterall, W. A. (1987) *Proc. Natl. Acad. Sci. U.S.A.* **84,** 5478–5482
5. Leung, A. T, Imagawa, T., and Campbell, K. P. (1987) *J. Biol. Chem.* **262,** 7943–7946
6. Ríos, E., Pizarro, G., and Stefani, E. (1992) *Annu. Rev. Physiol.* **54,** 109–133
7. Takeshima, H., Komazaki, S., Nishi, M., Iino, M., and Kangawa, K. (2000) *Mol. Cell* **6,** 11–22
8. Ma, H., Lou, Y., Lin, W. H., and Xue, H. W. (2006) *Cell Res.* **16,** 466–478
9. Nishi, M., Mizushima, A., Nakagawara, K., and Takeshima, H. (2000) *Biochem. Biophys. Res. Commun.* **273,** 920–927
10. Nishi, M., Sakagami, H., Komazaki, S., Kondo, H., and Takeshima, H. (2003) *Brain Res. Mol. Brain Res.* **118,** 102–110
11. Kakizawa, S., Moriguchi, S., Ikeda, A., Iino, M., and Takeshima, H. (2008) *Cerebellum* **7,** 385–391
12. Ito, K., Komazaki, S., Sasamoto, K., Yoshida, M., Nishi, M., Kitamura, K., and Takeshima, H. (2001) *J. Cell Biol.* **154,** 1059–1067
13. Komazaki, S., Ito, K., Takeshima, H., and Nakamura, H. (2002) *FEBS Lett.* **524,** 225–229
14. Landstrom, A. P., Kellen, C. A., Dixit, S. S., van Oort, R. J., Garbino, A., Weisleder, N., Ma, J., Wehrens, X. H., and Ackerman, M. J. (2011) *Circ. Heart Fail.* **4,** 214–223
15. Matsushita, Y., Furukawa, T., Kasanuki, H., Nishibatake, M., Kurihara, Y., Ikeda, A., Kamatani, N., Takeshima, H., and Matsuoka, R. (2007) *J. Hum. Genet.* **52,** 543–548
16. Minamisawa, S., Oshikawa, J., Takeshima, H., Hoshijima, M., Wang, Y., Chien, K. R., Ishikawa, Y., and Matsuoka, R. (2004) *Biochem. Biophys. Res. Commun.* **325,** 852–856
17. Xu, M., Zhou, P., Xu, S. M., Liu, Y., Feng, X., Bai, S. H., Bai, Y., Hao, X. M., Han, Q., Zhang, Y., and Wang, S. Q. (2007) *PLoS Biol.* **5,** e21
18. van Oort, R. J., Garbino, A., Wang, W., Dixit, S. S., Landstrom, A. P., Gaur, N., De Almeida, A. C., Skapura, D. G., Rudy, Y., Burns, A. R., Ackerman, M. J., and Wehrens, X. H. (2011) *Circulation* **123,** 979–988
19. Phimister, A. J., Lango, J., Lee, E. H., Ernst-Russell, M. A., Takeshima, H., Ma, J., Allen, P. D., and Pessah, I. N. (2007) *J. Biol. Chem.* **282,** 8667–8677
20. Lee, E. H., Cherednichenko, G., Pessah, I. N., and Allen, P. D. (2006) *J. Biol. Chem.* **281,** 10042–10048
21. Woo, J. S., Kim do, H., Allen, P. D., and Lee, E. H. (2008) *Biochem. J.* **411,** 399–405
22. Woo, J. S., Hwang, J. H., Ko, J. K., Kim do, H., Ma, J., and Lee, E. H. (2009) *Mol. Cell. Biochem.* **328,** 25–32
23. Li, H., Ding, X., Lopez, J. R., Takeshima, H., Ma, J., Allen, P. D., and Eltit, J. M. (2010) *J. Biol. Chem.* **285,** 39171–39179
24. Berbey, C., Weiss, N., Legrand, C., and Allard, B. (2009) *J. Biol. Chem.* **284,** 36387–36394
25. Zanou, N., Shapovalov, G., Louis, M., Tajeddine, N., Gallo, C., Van Schoor, M., Anguish, I., Cao, M. L., Schakman, O., Dietrich, A., Lebacq, J., Ruegg, U., Roulet, E., Birnbaumer, L., and Gailly, P. (2010) *Am. J. Physiol. Cell Physiol.* **298,** C149–C162
26. Hirata, Y., Brotto, M., Weisleder, N., Chu, Y., Lin, P., Zhao, X., Thornton, A., Komazaki, S., Takeshima, H., Ma, J., and Pan, Z. (2006) *Biophys. J.* **90,** 4418–4427
27. Lyfenko, A. D., and Dirksen, R. T. (2008) *J. Physiol.* **586,** 4815–4824
28. Stiber, J., Hawkins, A., Zhang, Z. S., Wang, S., Burch, J., Graham, V., Ward, C. C., Seth, M., Finch, E., Malouf, N., Williams, R. S., Eu, J. P., and Rosenberg, P. (2008) *Nat. Cell Biol.* **10,** 688–697
29. Park, C. Y., Shcheglovitov, A., and Dolmetsch, R. (2010) *Science* **330,** 101–105
30. Wang, Y., Deng, X., Mancarella, S., Hendron, E., Eguchi, S., Soboloff, J., Tang, X. D., and Gill, D. L. (2010) *Science* **330,** 105–109
31. Conti, A., Gorza, L., and Sorrentino, V. (1996) *Biochem. J.* **316,** 19–23
32. Collet, C., Csernoch, L., and Jacquemond, V. (2003) *Biophys. J.* **84,** 251–265
33. Jacquemond, V. (1997) *Biophys. J.* **73,** 920–928
34. Legrand, C., Giacomello, E., Berthier, C., Allard, B., Sorrentino, V., and Jacquemond, V. (2008) *J. Physiol.* **586,** 441–457
35. Cheng, H., Lederer, W. J., and Cannell, M. B. (1993) *Science* **262,** 740–744
36. Pouvreau, S., Csernoch, L., Allard, B., Sabatier, J. M., De Waard, M., Ronjat, M., and Jacquemond, V. (2006) *Biophys. J.* **91,** 2206–2215
37. Marty, I., Robert, M., Villaz, M., De Jongh, K., Lai, Y., Catterall, W. A., and Ronjat, M. (1994) *Proc. Natl. Acad. Sci. U.S.A.* **91,** 2270–2274
38. Mouton, J., Marty, I., Villaz, M., Feltz, A., and Maulet, Y. (2001) *Biochem. J.* **354,** 597–603
39. Vassilopoulos, S., Oddoux, S., Groh, S., Cacheux, M., Fauré, J., Brocard, J., Campbell, K. P., and Marty, I. (2010) *Biochemistry* **49,** 6130–6135
40. Murray, B. E., and Ohlendieck, K (1997) *Biochem. J.* **324,** 689–696
41. Serysheva, I. I. (2004) *Biochemistry* **69,** 1226–1232
42. Wang, Z. M., Messi, M. L., and Delbono, O. (2000) *Biophys. J.* **78,** 1947–1954